January 1999

The He-LiH potential energy surface revisited. I. An interpolated rigid rotor surface

Robert Hinde
University of Tennessee, rhinde@utk.edu

The He–LiH potential energy surface revisited. I. An interpolated rigid rotor surface

Brian K. Taylor and Robert J. Hinde
Department of Chemistry, University of Tennessee, Knoxville, Tennessee 37996-1600

(Received 9 September 1998; accepted 30 November 1998)

We reconsider the potential energy surface of the He–LiH system recently examined by Gianturco and co-workers [F. A. Gianturco *et al.*, Chem. Phys. **215**, 227 (1997)]. We compute the He–LiH interaction energy at the CCSD(T) level using large correlation consistent atomic basis sets supplemented with bond functions. To capture the severe anisotropy of the He–LiH potential, we interpolate our *ab initio* points in the angular direction with cubic splines, then expand the splines in terms of Legendre polynomials. The resulting smooth potential surface differs substantially from that of Gianturco *et al.*; in particular, our attractive He–LiH well is more than twice as deep as that of Gianturco *et al.*, with a He–LiH binding energy of $D_e = 176.7\ \mathrm{cm}^{-1}$. © *1999 American Institute of Physics.* [S0021-9606(99)30609-7]

I. INTRODUCTION AND BACKGROUND

The lithium chemistry of the early universe has recently been a topic of much interest in astrochemistry.[1–5] Processes involving the highly polar molecule LiH have been of particular interest. Because of its large dipole moment [$\mu = 5.88$ D (Ref. 6)], LiH exhibits several intense radiative rovibrational transitions;[3] thus emissions from rovibrationally excited LiH molecules may have played an important role in the radiative cooling of primordial gas clouds in the early universe.[7] Observation of the radiative emissions from excited LiH molecules could help quantify the lithium abundance in the primordial universe, allowing current models of big bang nucleosynthesis to be refined.[1] Finally, there has been some speculation that elastic scattering of low-energy blackbody photons from excited LiH molecules may have helped reduce the initial spatial anisotropy of the cosmic background radiation.[8]

Rovibrationally excited LiH molecules can be produced in the early universe either by radiative association of Li and H atoms or by inelastic collisions between ''cold'' LiH molecules and other constituents of the primordial universe. The possibility that excited LiH molecules produced via He–LiH collisions could play a role in the energy balance of the early universe motivated a recent study of the He–LiH potential energy surface (PES) by Gianturco and co-workers.[9,10] This study involved a spin-coupled valence bond treatment of the He–LiH electronic structure, using large atomic basis sets designed to describe the electrical properties of He and LiH accurately. The resulting PES differed substantially from an earlier PES computed by Silver[11] using third-order Møller–Plesset[12] theory (MP3); however, this is not very surprising given the relatively small basis set employed by Silver.

At a more fundamental level, the He–LiH system is of interest as a benchmark system for theoretical studies of both intermolecular potentials and collisional energy transfer. Because the He–LiH system has only six electrons, a wide variety of highly accurate methods can be used to treat the electronic structure of this system, and the theoretical *ab initio* PES for this system should be fairly close to the exact nonrelativistic Born–Oppenheimer PES. Furthermore, nearly exact computational studies of rotationally inelastic He–LiH collisions are feasible because of the large rotational constant of LiH and the small He–LiH reduced mass. Hence for this system we should expect very good agreement between experimental and fully *ab initio* cross sections for rotational energy transfer. If the *ab initio* He–LiH PES is accurate and the computational treatment of the collision dynamics is nearly exact, differences between the computed and experimental cross sections for He–LiH collisions can be interpreted in terms of non-Born–Oppenheimer effects, and can shed light on the role of these effects in collision processes.

Our initial interest in the He–LiH system was motivated by the extreme anisotropy of the underlying PES, which suggested that He–LiH collisions might exhibit interesting dynamics, thereby providing a stringent test of the ''angular momentum'' theory of rotational energy transfer developed by McCaffery and co-workers.[13,14] In this paper, we revisit the He–LiH PES using conventional supermolecular *ab initio* techniques coupled with large basis sets and a CCSD(T) (Ref. 15) treatment of electron correlation. Surprisingly, our PES differs significantly from that computed by Gianturco *et al.*;[9] we attribute this discrepancy to (1) differences in the basis sets used to compute the two surfaces and (2) differences in our treatment of the angular anisotropy of the surface.

The remainder of the paper is structured as follows. We begin by summarizing our computational techniques in Sec. II; there, we choose an appropriate level of *ab initio* theory for the He–LiH system and consider numerical methods for treating the angular anisotropy of this system's potential energy surface. In Sec. III, we construct a global rigid rotor *ab initio* PES for the He–LiH system. We then conclude with a brief discussion in Sec. IV. A subsequent paper[16] describes a fully three-dimensional He–LiH PES in which the LiH bond length is allowed to change.

TABLE I. Computed LiH zero point energies (ZPEs) and excitation energies for selected $(v,j)\rightarrow(v',j')$ rovibrational transitions. All energies are given in cm^{-1}. Experimental values are taken from Ref. 22 and have been corrected to eliminate non-Born–Oppenheimer effects.

Energy	MP2	MP4	CCSD(T)	Expt.
ZPE	711.07	701.94	696.41	696.89
(0,0)→(0,1)	14.85	14.78	14.73	14.82
(0,1)→(0,2)	29.67	29.54	29.45	29.65
(0,2)→(0,3)	44.47	44.27	44.12	44.47
(0,0)→(1,0)	1389.53	1368.52	1355.95	1359.18
(1,0)→(2,0)	1347.62	1324.72	1310.35	1314.22
(2,0)→(3,0)	1307.21	1282.50	1266.10	1268.99

TABLE II. Electrical properties of isolated LiH and He monomers in atomic units (polarizability: 1 a.u. = 1.4818×10^{-31} m^3; dipole moment: 1 a.u. = 8.4784×10^{-30} C m).

Property	MP2	MP4	CCSD(T)	Literature value
He α	1.357	1.378	1.381	1.383 ± 0.001[a]
LiH $\alpha_\perp$	26.86	28.47	29.47	30.9 ± 0.4[b]
LiH $\alpha_\parallel$	23.61	24.96	26.03	24.6 ± 0.4[b]
LiH $\mu(v=0)$	2.349	2.331	2.320	2.314 ± 0.001[c]

[a]Experimental value (Ref. 24).
[b]Diffusion quantum Monte Carlo value (Ref. 25).
[c]Experimental value (Ref. 6).

II. COMPUTATIONAL METHODS

A. *Ab initio* calculations: Monomer properties

We begin this section by discussing our choice of basis set, which combines a large set of atom-centered Gaussian functions with a small set of Gaussian bond functions. The atom-centered basis set we use consists of a $(6s3p2d)/[4s3p2d]$ aug-cc-pVTZ basis set for hydrogen,[17] a $(7s3p2d)/[4s3p2d]$ aug-cc-pVTZ basis set for helium,[18] and a truncated $(12s6p3d2f)/[5s4p3d2f]$ cc-pVQZ basis set (which omits g orbitals) for lithium.[19] This atom-centered basis set was supplemented with a $(3s3p2d)$ set of Gaussian orbitals located along the He–LiH bond, which we discuss in more detail below. The exponents of the bond functions were taken from Ref. 20.

To test the adequacy of the atom-centered basis set, we computed various properties of the isolated He and LiH monomers. First, we computed the total energy of LiH as a function of bond length r over the interval $0.90\ \text{Å}\leqslant r\leqslant 2.75\ \text{Å}$ in steps of 0.05 Å . These calculations were performed at the MP2, MP4 and CCSD(T) levels. We fit these energies to a cubic spline and used the Numerov–Cooley method[21] to compute rovibrational wave functions and energy levels for LiH. Table I lists the zero point energy for each LiH potential curve, as well as excitation energies from the rovibrational ground state to selected low-lying (v,j) levels. The CCSD(T) calculations give fairly good agreement with experimental values that have been corrected for non-Born–Oppenheimer effects.[22]

We also compared our CCSD(T) LiH potential curve against the experimentally determined Born–Oppenheimer potential curve.[22] The minimum of the CCSD(T) curve is at $r=1.5996$ Å . When our CCSD(T) curve is shifted inward by 0.0047 Å to place its minimum at the experimental r_{eq}, the CCSD(T) curve and the experimental curve agree to better than 1% for energies below $10^4\ cm^{-1}$.

Next, we computed some electrical properties of isolated LiH and He. Using the finite-field perturbation technique with an external electric field of 0.001 atomic units, we evaluated the polarizabilities of He and of LiH (using the equilibrium LiH bond length[23] $r_{eq}=1.5949$ Å) at the MP2, MP4, and CCSD(T) levels. We also computed the dipole moment $\mu(r)$ of LiH across the interval $0.9\ \text{Å}\leqslant r\leqslant 2.7\ \text{Å}$ in steps of 0.1 Å, fit these dipole moments to a cubic spline, and estimated the dipole moment of the LiH rovibrational ground state by integrating $\mu(r)$ over the ground state probability density for LiH. Table II summarizes our results; our CCSD(T) calculations are again in good agreement with values obtained from experiment[6,24] and from diffusion quantum Monte Carlo studies.[25]

B. *Ab initio* calculations: Interaction energies

With a suitable basis set for the LiH and He monomers in hand, we now consider the He–LiH interaction potential, which is dominated by induction and dispersion forces. A number of research groups have studied the use of bond functions to improve the *ab initio* description of van der Waals dispersion forces in a computationally efficient manner.[20,26–31] In this section, we investigate the application of bond functions to the He–LiH system.

First we describe the computational approach we use to evaluate the He–LiH interaction energy. In all of our calculations, we employ the Boys–Bernardi full counterpoise method.[32] This requires three separate *ab initio* calculations—one for the He–LiH supermolecule, one for He, and one for LiH—each of which uses a basis set consisting of both the atom-centered orbitals of all three atoms and any bond functions. These calculations are performed in the conventional Jacobi coordinate system (R,θ), where R is the length of the vector connecting the LiH center of mass and the He atom and θ is the angle between this vector and the LiH bond. The collinear LiH–He geometry corresponds to $\theta=0°$. The LiH bond length is fixed at its equilibrium value r_{eq}. The masses of ^{7}Li and ^{1}H are used to determine the LiH center of mass.

When bond functions are used, we place them on the line which connects the He atom with the LiH center of mass, midway between the He atom and the intersection of this line with a circle which has the LiH bond as its diameter. This procedure is necessary to prevent computational linear dependence of the bond functions and the hydrogen-centered orbitals at $\theta=0°$ and small R.

For bond functions to improve the description of intermolecular dispersion forces in a reliable fashion, the atom-centered basis set used for monomer calculations must be nearly saturated at the Hartree–Fock (HF) level, so that introduction of the bond functions does not appreciably change the HF interaction energy.[20] To check the saturation of our atom-centered basis set, we compute the Hartree–Fock He–LiH interaction energy both with and without the bond functions; the results are shown in Table III for a point near the global minimum on the He–LiH PES.

TABLE III. Basis set dependence of the interaction energy $V(R,\theta)$ at $R=2.3$ Å and $\theta=180°$. All energies are given in μhartrees. CCSD(T) calculations which failed to converge are denoted by NC.

Atomic basis set[a]	Bond functions	HF	MP2	MP4	CCSD(T)
A	None	−479.55	−623.26	−646.02	−630.83
A	$(3s3p2d)$	−563.23	−787.75	−808.64	NC
B	None	−539.63	−713.38	−743.39	−735.93
B	$(3s3p2d)$	−557.90	−771.01	−800.51	−793.73
C	None	−560.77	−762.33	−794.82	−787.41
C	$(3s3p2d)$	−558.52	−778.36	−807.72	−800.73
C′	None	−558.15	−757.59	−789.92	−775.14
C′	$(3s3p2d)$	−558.60	−777.43	−806.78	−799.65
C′	$(3s3p2d1f)$	−558.29	−777.33	−806.86	−799.83
C′	$(5s5p4d)$	−558.94	−780.10	−808.63	NC
C′	$(3s3p)$	−560.04	−770.84	−801.48	−794.13
D	None	−559.33	−769.62	−800.87	NC
D	$(3s3p2d)$	−559.94	−779.05	−809.93	NC
D′	None	−558.45	−767.34	−798.36	−791.80
D′	$(3s3p2d)$	−559.85	−778.52	−809.35	−803.03

[a]A is the basis set used by Gianturco *et al.* (Ref. 9); B is a basis set consisting of aug-cc-pVTZ on H and He and cc-pVTZ on Li; C is a basis set consisting of aug-cc-pVTZ on H and He and cc-pVQZ on Li; D is a basis set consisting of aug-cc-pVQZ on H and He and cc-pVQZ on Li. Basis sets C′ and D′ are obtained from C and D by omitting the Li g functions.

This table shows that with our atom-centered basis set (listed as C′ in Table III), the HF interaction energy of He–LiH changes by less than 0.5 μhartrees when the bond functions are added. If we use smaller atom-centered basis sets (including that employed by Gianturco *et al.*,[9] listed as A in Table III), we observe substantial changes in the HF interaction energy when bond functions are added, suggesting that smaller basis sets give an inadequate description of He–LiH interactions at the Hartree–Fock level.

The deficiencies of smaller basis sets are magnified when correlated *ab initio* methods are used; the HF binding energy obtained using basis set C′ is about 80 μhartrees larger than that obtained using basis set A, while at the CCSD(T) level, basis set C′ predicts a binding energy which is 145 μhartrees larger than that predicted by basis set A.

Correlated calculations also underscore the need to use bond functions to obtain accurate He–LiH interaction energies: with atom-centered basis set C′, the addition of bond functions increases the CCSD(T) He–LiH binding energy by 25 μhartrees. Even when larger atom-centered basis sets are used for hydrogen and helium (basis set D′ in Table III), bond functions contribute another 10 μhartrees (or 2 cm^{-1}) to the CCSD(T) He–LiH binding energy. Note, however, that when bond functions are used, the CCSD(T) binding energies computed using basis sets C′ and D′ differ by less than 3 μhartrees, suggesting that the combination of atom-centered basis set C′ and a set of $(3s3p2d)$ bond functions is close to the complete basis set limit.

We also point out that basis sets B and D are consecutive members of a correlation-consistent sequence. Although basis set B is not saturated at the Hartree–Fock level, it gives near-HF results when supplemented with bond functions. If we then compare the MP4 He–LiH interaction energy for basis sets B and D (using bond functions in both cases), we see that the He–LiH binding energy changes by less than 10 μhartrees on going from the triple-zeta to the quadruple-zeta level. Because of the convergence properties of correlation-consistent basis set sequences,[33–35] we anticipate that further extension of the basis set will produce very small changes in the He–LiH binding energy. But as Table III shows, basis sets C and D give similar results when bond functions are used, indicating that a triple-zeta treatment of H and He is adequate provided bond functions are used. Finally, omission of the single Li g function from the cc-pVQZ basis set does not change the He–LiH binding energy significantly; this omission accelerates the CCSD(T) calculations considerably by permitting storage of the two-electron integrals on disk. All of our ''production'' calculations described in Sec. III were performed using basis set C′ and a set of $(3s3p2d)$ bond functions.

As a check on the adequacy of our bond functions, we performed some test calculations with larger sets of bond functions. First we added a single f orbital (with exponent 0.3) to the set of bond functions to generate a $(3s3p2d1f)$ bond function set; then we supplemented the original bond functions with additional diffuse and compact s, p, and d orbitals (with exponents computed in an even-tempered fashion) to generate a $(5s5p4d)$ bond function set. The results obtained using these extended bond function sets were very close to those obtained using the original $(3s3p2d)$, which suggests that our bond function space is also near saturation. Moving the bond functions in or out by 0.1 Å changes the CCSD(T) interaction energy by less than 1 μhartree, so that the precise placement of the bond functions does not seem to be critical.

All of the *ab initio* calculations described in this subsection were performed with GAUSSIAN 94 (Ref. 36) using Cartesian d and f orbitals; no frozen core approximation was used in the correlated calculations. Cartesian d and f orbitals were used to permit comparison between the GAUSSIAN 94 results and computations using GAMESS,[37] as described in Sec. III.

C. Fitting techniques

The He–LiH PES is very anisotropic, in part because the large mass imbalance between lithium and hydrogen places the LiH center of mass very close to the lithium atom, and in part because the LiH electronic structure resembles a Li^+H^- ion pair state with a very anisotropic electron density distribution. Figure 1 shows the CCSD(T) He–LiH potential energy V as a function of θ at $R=2.15$ Å , which is close to the He–LiH distance at the global minimum on the PES. We now discuss numerical methods for fitting a PES with this shape.

Ideally, we would like to fit $V(\theta)$ to an analytic function which reproduces the low-energy data (below, say, $V=0.5$ eV) to an accuracy of 1 cm^{-1}. This goal may seem to be a rather stringent requirement. However, we believe that our *ab initio* calculations are accurate to within 1–2 cm^{-1} (see Table III), so our PES should preserve this accuracy if possible. Furthermore, experiments routinely measure the bound state energies of van der Waals molecules to sub-cm^{-1} precision; our PES can serve as a reliable guide to these energies only if it is accurate to within 1 cm^{-1} or better in the potential's attractive region.

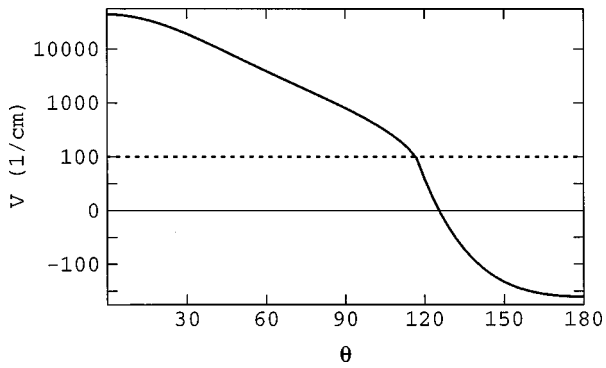

FIG. 1. He–LiH interaction energy as a function of θ at $R=2.15$ Å . Note that the plot is logarithmic for $V>100$ cm^{-1}.

The conventional approach to this fitting problem is to expand $V(\theta)$ in terms of Legendre polynomials,

$$V(\theta)=\sum_{n=0}^{\infty} c_n P_n(\cos\ \theta) \tag{1}$$

with

$$c_n=\frac{2n+1}{2}\int_0^{\pi} V(\theta)P_n(\cos\ \theta)\sin\ \theta \mathrm{d}\theta. \tag{2}$$

If $V(\theta)$ is known at the N Gauss–Legendre quadrature nodes which exactly integrate polynomials of degree $2N-1$, estimates of the first N coefficients in this infinite series can be obtained using numerical quadrature,

$$\tilde{c}_n=\frac{2n+1}{2}\sum_{i=1}^{N} w_i V(\theta_i)P_n(\cos\ \theta_i)\approx c_n, \tag{3}$$

where $\{\theta_i\}$ are the quadrature nodes and $\{w_i\}$ are the corresponding weights. The potential $V(\theta)$ can then be represented as a truncated sum of Legendre polynomials using the N approximate coefficients $\{\tilde{c}_n\}$,

$$V(\theta)\approx\sum_{n=0}^{N-1} \tilde{c}_n P_n(\cos\ \theta). \tag{4}$$

This approach will succeed when the coefficients $\{c_k : k \geqslant N\}$ are small compared with the leading N coefficients in Eq. (1). If this is not the case, the approximation represented by Eq. (4) will be inaccurate, both because the sum has been truncated too early and because the approximate coefficients $\{\tilde{c}_n\}$ will differ substantially from the exact coefficients $\{c_n\}$.

Table IV shows the root mean square and maximum absolute deviation between the potential $V(\theta)$ shown in Fig. 1 and the truncated sum of Eq. (4), as a function of the number N of approximate coefficients included in the sum. [Only points with $V(\theta)<0.5$ eV are used in constructing this table.] We see that for $N<23$, Eq. (4) does not reproduce the low-energy portion of the potential to within 1 cm^{-1} accuracy. The maximum absolute deviation between Eq. (4) and the low-energy portion of the exact potential occurs at $\theta=180°$; Table IV shows that the value of $V(180°)$ predicted by Eq. (4) converges rather slowly to the exact value as N increases.

A spline-based representation of $V(\theta)$ gives equally good results using fewer *ab initio* calculations. Suppose that we compute $V(\theta)$ at N equally spaced angles from $\theta=0°$ to $\theta=180°$ and fit a cubic spline through these points. Table IV shows the deviation between this spline and the potential $V(\theta)$ shown in Fig. 1, again as a function of N. The spline-based interpolant consistently outperforms the Legendre polynomial expansion; the deviation of the cubic spline from $V(\theta)$ is typically two to three times smaller than that of a truncated Legendre polynomial expansion with the same value of N. Consequently, fewer *ab initio* calculations are required to approximate $V(\theta)$ to within 1 cm^{-1} accuracy: the cubic spline achieves this goal at $N=19$, as compared with $N=23$ for Eq. (4).

TABLE IV. Root mean square deviation Δ_{rms} and maximum absolute deviation Δ_{max} (both in cm^{-1}) between the potential $V(\theta)$ shown in Fig. 1 and either the quadrature-based approximation given by Eq. (4) or the spline-based approximation described in the text. Also shown is the potential $V(180°)$ (in cm^{-1}) at $\theta=180°$ predicted by Eq. (4); the actual potential at $\theta=180°$ is -160.53 cm^{-1}. N is either the number of approximate coefficients in Eq. (4) or the number of points used to construct the spline-based approximation. Only points with $V(\theta)<0.5$ eV are considered in computing the deviations Δ_{rms} and Δ_{max}.

	Eq. (4)			Spline	
N	Δ_{rms}	Δ_{max}	$V(180°)$	Δ_{rms}	Δ_{max}
12	4.44	12.58	−173.11	1.41	10.04
18	0.82	2.56	−163.09	0.21	1.09
19	0.65	2.16	−158.36	0.17	0.80
20	0.52	1.74	−162.27	0.16	0.76
21	0.41	1.39	−159.14	0.11	0.64
22	0.30	1.06	−161.59	0.09	0.41
23	0.23	0.82	−159.71	0.09	0.39

A cubic spline representation of $V(\theta)$ is cumbersome for use in rotational scattering calculations; however, the spline can in principle be approximated by a Legendre polynomial expansion to whatever accuracy is desired. A spline-based interpolation of $V(\theta)$ thus provides us with a method for generating potential surfaces with accuracies comparable to conventional high-order Legendre polynomial expansions, but which require fewer *ab initio* calculations. We also note that by locating spline nodes in strategic locations (such as $\theta=180°$) we can improve the accuracy of the PES in ''important'' regions.

To make an even more compelling case for the use of cubic splines to represent $V(\theta)$, we briefly examine the angular dependence of the He–LiH PES at different levels of *ab initio* theory. Let V_{MP2} represent the counterpoise-corrected He–LiH interaction energy, calculated at the MP2 level of theory using basis set C′ and the $(3s3p2d)$ set of bond functions described above. Then define $V_c=V-V_{\mathrm{MP2}}$ to be the difference between the CCSD(T) interaction potential and V_{MP2}. Figure 2 shows how V_{MP2} and V_c depend on θ at $R=2.15$ Å . The large-scale anisotropy shown in Fig. 1 is already present at the MP2 level of theory; in comparison, the ''correction'' term V_c is one to two orders of magnitude smaller than V_{MP2}. This observation suggests that we might be able to represent $V(\theta)$ faithfully and efficiently by sampling V_{MP2} at several closely spaced angles while evaluating V_c on a much coarser angular grid. Such an approach is attractive because MP2 calculations are much quicker than CCSD(T) calculations.

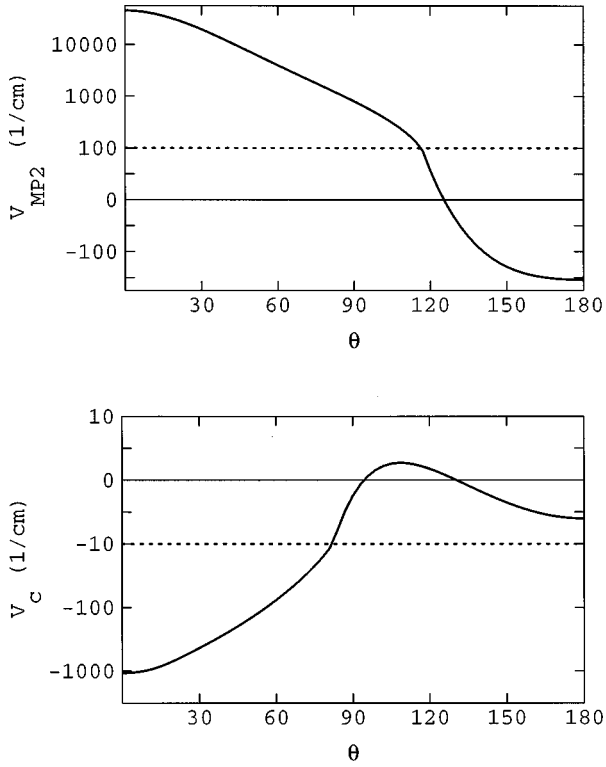

FIG. 2. V_{MP2} and V_c as a function of θ at $R=2.15$ Å . Note that the plots are logarithmic for $V_{MP2}>100$ cm^{-1} and for $V_c<-10$ cm^{-1}.

We test this hypothesis by computing V_{MP2} at several equally spaced points between $\theta=0°$ and $\theta=180°$ and constructing a cubic spline through these points. Next, we compute V_c on a coarser grid of equally spaced points, again between $\theta=0°$ and $\theta=180°$, and pass a second cubic spline through these points. We then compare $V(\theta)$ with the sum of the two splines. The results of this ''dual spline'' approach are shown in Table V as a function of s_{MP2} and s_c, which are the respective spacings (in degrees) between V_{MP2} and V_c spline nodes. We see that a reliable approximation to $V(\theta)$ can be obtained using either $s_{MP2}=10°$ and $s_c=15°$ or $s_{MP2}=5°$ and $s_c=20°$; a choice between these two dual spline schemes depends on the relative speed of MP2 and CCSD(T) *ab initio* calculations, which is to some degree software- and hardware-dependent.

Previous studies of the He–LiH PES (Refs. 9,11) have attempted to capture the anisotropy of this surface by computing the interaction energy (for fixed R) at twelve angles. Table IV shows that this approach is inadequate at small R; sampling the potential at only twelve angles introduces substantial errors into the surface, whether Legendre polynomials or splines are used to fit the angular dependence of the PES. Consequently, the surfaces presented in Refs. 9 and 11 should be used with caution.

TABLE V. Root mean square and maximum absolute deviation (both in cm^{-1}) between the potential $V(\theta)$ shown in Fig. 1 and the dual spline approximation described in the text. Only points with $V(\theta)<0.5$ eV are considered in computing these deviations. The spacing in degrees between V_{MP2} spline nodes is s_{MP2} and the spacing in degrees between V_c spline nodes is s_c. The first entry in each block is the root mean square deviation; the second entry is the maximum absolute deviation.

s_{MP2}	$s_c=10°$	$s_c=15°$	$s_c=20°$	$s_c=30°$
5°	0.01/0.06	0.09/0.38	0.30/0.99	1.17/3.23
10°		0.12/0.44	0.43/1.72	1.29/3.61
15°			0.75/3.03	1.60/5.30

III. GLOBAL SURFACE

We have used the dual spline approach described above to obtain a global PES for the He–LiH system. We begin this section with a brief outline of our treatment of the radial coordinate R. We then discuss some of the interesting features of the PES and present the results of several tests designed to assess the accuracy of our interpolation scheme. Finally, we compare our surface with those presented in Refs. 9 and 11.

We employ a radial grid of R values extending from $R=2.5\ a_0$ to $R=12\ a_0$. In the range $2.5\ a_0 \leqslant R \leqslant 9\ a_0$, we use a grid spacing of $\Delta R=0.25\ a_0$; for $9\ a_0 \leqslant R \leqslant 12\ a_0$, we use $\Delta R=0.5\ a_0$. At each R value in this grid, we compute $V(R,\theta)$ using the dual spline approach. For $R \leqslant 4\ a_0$, where the anisotropy of the PES is particularly large, we evaluate V_c every 15 degrees, while for $R>4\ a_0$ we evaluate V_c every 30 degrees. At each R value, V_{MP2} is computed every 10 degrees. We use GAUSSIAN 94 (Ref. 36) to calculate V_c and GAMESS (version dated 31 October 1996) (Ref. 37) to calculate V_{MP2}.

When the He atom is very close to the hydrogen end of LiH, we encounter difficulties with the *ab initio* calculations due to computational linear dependence of the basis set. This problem arises at $R<4.25\ a_0$ and $\theta \leqslant 30°$ for MP2 calculations and at $R<5.5\ a_0$ and $\theta \leqslant 30°$ for CCSD(T) calculations. The PES at these points is extremely repulsive, and the precise value of the potential is not important for, e.g., low-energy scattering calculations. However, we must define V_{MP2} and V_c at these points in order to implement our dual spline approach.

We are able to calculate V_{MP2} and V_c at some of these geometries by eliminating the bond function from our basis set. At those points where even this reduced basis set is computationally linearly dependent, we arbitrarily set V_{MP2} to 10^5 cm^{-1}. We also replace any computed values of V_{MP2} which exceed 10^5 cm^{-1} with this value to prevent unphysical ''dips'' in the surface near $\theta=0°$ and to reduce the number of Legendre polynomials needed to represent the splined potential surface. At geometries where V_c cannot be calculated, we extrapolate V_c along each constant-R arc to small angles using $V_c(\theta)=A+B\theta^2$. The values of A and B are computed for each arc by fitting this functional form to the V_c values at the two smallest angles θ for which V_c can be calculated. We emphasize that our use of spline interpolation insures that these computational ''tricks'' do not materially alter the shape of the PES at energies of interest (say, $V<0.5$ eV).

Once the PES is defined along each constant-R arc, we expand the potential at each R value in terms of Legendre polynomials,

$$V(R,\theta)=\sum_{n=0}^{J_{max}} c_n(R)P_n(\cos\ \theta); \tag{5}$$

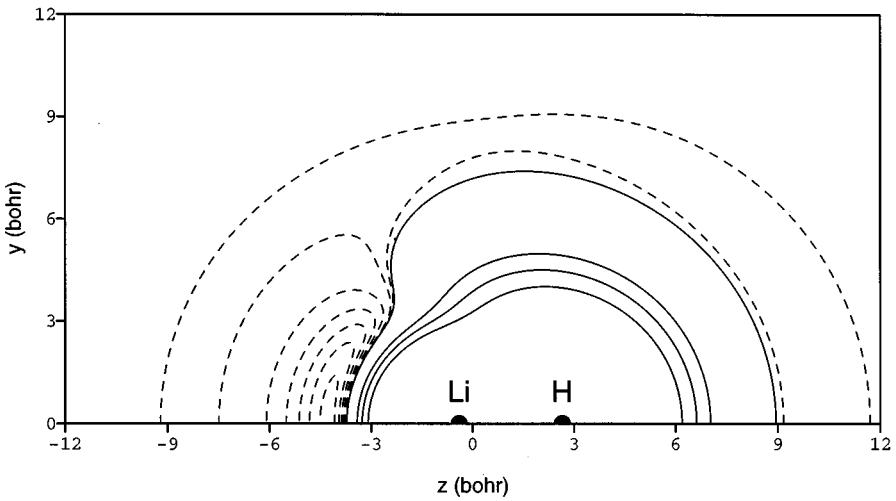

FIG. 3. Contour plot of the He–LiH PES. Dashed lines indicate energies from -165 cm^{-1} to -15 cm^{-1} in steps of 30 cm^{-1}, and the energy -5 cm^{-1}; solid lines indicate energies of 0 cm^{-1}, 500 cm^{-1}, 1000 cm^{-1}, and 2000 cm^{-1}.

the coefficients $\{c_n(R)\}$ are evaluated as in Eq. (3) using 10^4-point trapezoid rule quadrature. At each R value, $J_{\max}$ is chosen so that the Legendre polynomial expansion fits the dual spline potential to within 1 cm^{-1} for $V<1$ eV; $J_{\max}$ ranges from 34 at $R=2.5\ a_0$ to 4 at $R=12\ a_0$.

Finally, the coefficients $\{c_n(R)\}$ are interpolated using cubic splines to extend the PES to arbitrary R values. Beyond $R=12\ a_0$, the coefficients $\{c_n(R):0\leqslant n\leqslant 4\}$ are extrapolated according to $c_n(R)=A_nR^{-\beta_n}$; the parameters A_n and β_n are computed from the value of c_n at the two largest R values.

Figure 3 is a contour plot of the final PES. The surface is dominated by an attractive well 176.7 cm^{-1} deep at the linear He–LiH geometry with $R=4.25\ a_0$. For angles $\theta<90°$, the He–LiH interaction is almost entirely repulsive, with only a very shallow (9.8 cm^{-1} deep) ''trough'' at $R\approx 10\ a_0$. The shape of the PES reflects the electronic structure of the LiH molecule, which can be viewed as a Li^+H^- ion pair state. When the He atom is near the lithium end of LiH, it is strongly attracted to the compact Li^+ core under the influence of induction forces. In principle, these same forces are active at the hydrogen end of LiH; here, however, Pauli repulsion between the He atom and the diffuse H^- electron cloud forces the He atom to remain far away from LiH, where induction forces are substantially weaker.

We test the global accuracy of our fit by comparing the He–LiH interaction energy predicted by our PES with *ab initio* results at randomly selected points. We selected 282 random points (R,θ) in a 3 a_0 wide band extending out from the $V=2000$ cm^{-1} contour line predicted by our surface. This selection scheme concentrates points in the area of most interest, bypassing both the highly repulsive region which is less relevant for low-energy scattering calculations and the long-range, weakly anisotropic region which is easily fit by simple functional forms. Table VI shows how the energies predicted by our surface differ from the *ab initio* CCSD(T) values; we see that our PES agrees very well with these *ab initio* calculations.

As a further test of the reliability of our PES, we investigate the accuracy of the four repulsive contour lines shown in Fig. 3. Along each of these contour lines, we perform a CCSD(T) calculation of the He–LiH interaction energy at 10° intervals. We find that along the three positive energy contours, the *ab initio* energy differs by 1% or less from the predicted contour energy; along the $V=0$ cm^{-1} contour, the deviation between the fitted surface and the *ab initio* results is less than 0.5 cm^{-1}. The greatest deviation is typically in the region $120°\leqslant\theta\leqslant 180°$ where the interaction energy rises very rapidly as R decreases; because the repulsive wall is steep here, small errors in the positions of the predicted contour lines lead to relatively large differences between the predicted and *ab initio* interaction energy. The fact that these differences amount to less than 1% of the He–LiH potential, like the results presented in Table VI, indicates that our PES is a faithful representation of the underlying CCSD(T) potential.

Our PES has a substantially deeper He–LiH well than do the surfaces presented in Refs. 9 and 11. Figure 4(a) shows $V(R)$ for the three surfaces along the ray $\theta=169°$. (This is the angle nearest 180° for which *ab initio* results from Ref. 9 are available.) At large R, the He–LiH PES is dominated by induction and dispersion forces. The induction contribution to the PES can be closely approximated by $V_{\rm ind}(R,\theta)=-\alpha[\mathbf{E}(R,\theta)]^2/2$, where α is the polarizability of He and $\mathbf{E}(R,\theta)$ is the electric field at (R,θ) arising from the LiH charge distribution. With GAUSSIAN 94, we have evaluated $\mathbf{E}(R,\theta=169°)$ at the CCD(full) level using basis set C′; we then used these results (and the experimental polarizability of He) to compute $V_{\rm ind}(R,\theta=169°)$. The results are shown

TABLE VI. Root mean square, average absolute, and maximum absolute deviation (all in cm^{-1}) between our dual spline fit and CCSD(T) *ab initio* calculations at 282 randomly selected points (R,θ) chosen as described in the text. The points are divided into four energy strata so that the accuracy of our PES at low and high energies can be compared.

Energy range (cm^{-1})	$\Delta_{\rm rms}$	$\Delta_{\rm avg}$	$\Delta_{\max}$	Number of points
1000–2000	5.67	1.79	19.65	44
500–1000	1.52	0.99	4.46	45
0–500	0.84	0.67	4.09	132
<0	0.15	0.29	0.58	61

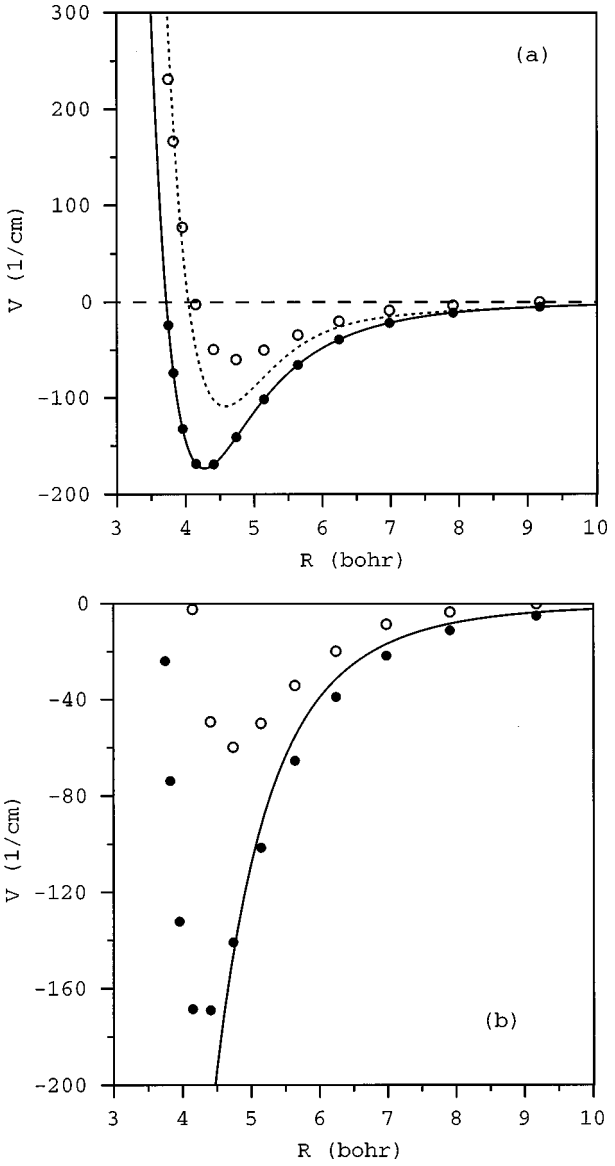

FIG. 4. (a) The radial potential $V(R)$ at $\theta=169°$ for three He–LiH surfaces. The filled circles represent our single-point CCSD(T) calculations, and the solid line is the dual spline interpolating surface presented here. The open circles are the *ab initio* results of Ref. 9, and the dotted line is the analytic fit presented in Ref. 11. (b) Comparison of our single-point CCSD(T) calculations (filled circles), the *ab initio* results of Ref. 9 (open circles), and the induction potential V_{ind} (solid line) at $\theta=169°$.

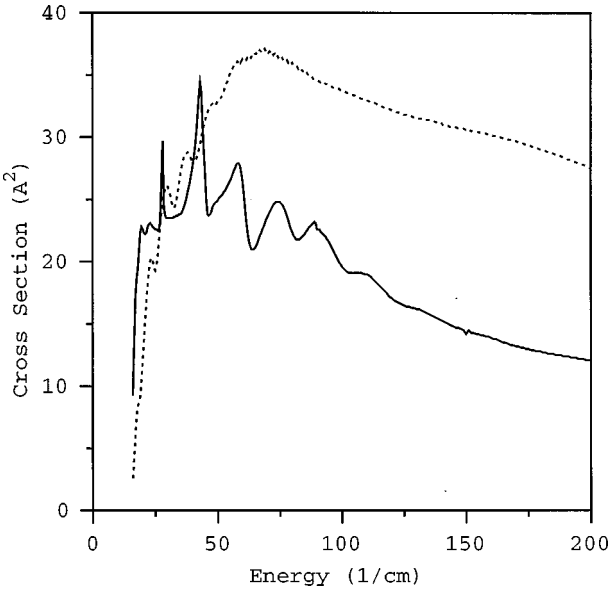

FIG. 5. Low-energy close-coupled $j=0\rightarrow1$ cross sections obtained using the potential surface presented here (solid line) and that presented in Ref. 11 (dotted line).

in Fig. 4(b). This figure shows that our *ab initio* energies agree rather well with the energies predicted by this induction-only model; our *ab initio* results are slightly more attractive than V_{ind} because they also include the effects of dispersion forces. Conversely, the PES of Ref. 9 is substantially less attractive than V_{ind}.

The differences among the three potential surfaces are large enough that they should be readily evident in experimental observables, such as rotational energy transfer cross sections for He–LiH collisions or the rovibrational energy level pattern of He–LiH van der Waals complexes. Because we treated the LiH molecule as a rigid rotor in our calculations, our PES cannot serve as a reliable guide to the rovibrational energy levels of He–LiH complexes. We can, however, compare (rigid rotor) rotational scattering cross sections obtained using the three surfaces, thereby gaining some insight into the dynamical effects of the differences seen in Fig. 4. Unfortunately, the fitted PES presented in Ref. 9 exhibits spurious attractive wells at small R, which we felt might taint the cross sections obtained using this surface; consequently, we did not perform rotational scattering calculations using this PES.

Figure 5 shows close-coupled low-energy $j=0\rightarrow1$ integral cross sections [computed using Hibridon 4.0.1 (Refs. 38–40)] for He–LiH collisions on our PES and on the surface presented by Silver.[11] The cross sections obtained using Silver's PES are substantially larger than those obtained using the PES presented here. We believe that this is because the repulsive wall of Silver's PES is shifted outward to larger R values [see Fig. 4(a)], so that for this surface the LiH ''target'' appears larger to the incoming He atom.

We stress that the results shown in Fig. 5 are for collisions in which the LiH molecule behaves as a rigid rotor. Although LiH $v=0\rightarrow1$ transitions are impossible at the low collision energies considered here, slight differences between the interaction of He atoms with ''frozen'' LiH and with $v=0$ LiH could change the cross sections shown in Fig. 5 somewhat. Hence a full three-dimensional PES is needed to draw definitive conclusions about the role of He–LiH collisions in the energetics of the primordial universe; we will present such a surface elsewhere.[16]

IV. SUMMARY AND CONCLUSIONS

We have carried out extensive supermolecular *ab initio* calculations of the He–LiH potential surface, using large basis sets and a CCSD(T) treatment of electron correlation. The He–LiH potential is very anisotropic, and special numerical methods are required to develop an analytic fit of the *ab initio* calculations without introducing spurious features into the potential surface. Spline-based interpolation of our

single-point CCSD(T) calculations gives a smooth rigid rotor PES $V(R,\theta)$ in which the LiH bond length is fixed at its equilibrium value. Several tests of the surface indicate that it is a faithful representation of the *ab initio* CCSD(T) potential and that it accurately reproduces the severe angular anisotropy of the He–LiH system. At large R, our PES also agrees very well with the asymptotic He–LiH induction potential.

Our surface predicts the He–LiH binding energy D_e to be 176.7 cm^{-1}; this binding energy is substantially larger than that obtained by either Gianturco *et al.*[9] or Silver[11] in their studies of the He–LiH system. We attribute these discrepancies to two factors. First, the basis set used in the present work is significantly larger than that used by Gianturco *et al.* or by Silver; these large basis sets are required to compute the He–LiH interaction energy at even the Hartree–Fock level. Second, we take special care to accurately model the angular anisotropy of the He–LiH PES. In Refs. 9 and 11, the angular variation of the He–LiH potential was treated by sampling the PES at twelve angles; the results presented here (see Table IV) suggest that finer sampling in the angular direction is needed to represent the anisotropy of the He–LiH surface at small R values.

Experimental studies of low-energy He–LiH collisions would help determine which of these potential surfaces is most accurate. Unfortunately, the only published measurements of He–LiH scattering cross sections[41] have large error bars and represent averages over a wide spread of translational energies. Perhaps our results will stimulate further experimental studies of this astrophysically important system.

Note added in proof. The *ab initio* calculations on which our potential energy surface is based can be obtained through the E-PAPS service.[42]

ACKNOWLEDGMENTS

Some basis sets were obtained from version 1.0 of the Extensible Computational Chemistry Environment Basis Set Database, which was developed and distributed by the Molecular Science Computing Facility at Pacific Northwest National Laboratory's Environmental and Molecular Sciences Laboratory (http://www.emsl.pnl.gov/). We would like to thank Professor K. Peterson and the authors of Ref. 19 for providing us with basis sets from this paper prior to publication. We also thank Professor F. Gianturco for providing us with the *ab initio* calculations used to construct the He–LiH surface in Ref. 9. The comments of an anonymous referee improved the clarity of our presentation. This work was partially supported by the National Science Foundation through Grant No. CHE-9528318, awarded in 1995. Publication of this work was supported by the Exhibit, Performance, and Publication Expense fund of the UTK Office of Research.

[1] M. Signore, G. Vedrenne, P. de Bernardis, V. Dubrovich, P. Encrenaz, R. Maoli, S. Masi, G. Mastrantonio, B. Melchiorri, F. Melchiorri, and P. E. Tanzailli, Astrophys. J., Suppl. Ser. **92**, 535 (1994).
[2] A. Dalgarno, K. Kirby, and P. C. Stancil, Astrophys. J. **458**, 397 (1996).
[3] P. C. Stancil, S. Lepp, and A. Dalgarno, Astrophys. J. **458**, 401 (1996).
[4] F. A. Gianturco, P. Gori Giorgi, H. Berriche, and F. X. Gadea, Astron. Astrophys., Suppl. Ser. **117**, 377 (1996).
[5] P. C. Stancil and A. Dalgarno, Astrophys. J. **479**, 543 (1996).
[6] L. Wharton, L. P. Gold, and W. Klemperer, J. Chem. Phys. **37**, 2149 (1962).
[7] S. Lepp and J. M. Shull, Astrophys. J. **280**, 465 (1984).
[8] R. Maoli, F. Melchiorri, and D. Tosti, Astrophys. J. **425**, 372 (1994).
[9] F. A. Gianturco, S. Kumar, S. K. Pathak, M. Raimondi, M. Sironi, J. Gerratt, and D. L. Cooper, Chem. Phys. **215**, 227 (1997).
[10] F. A. Gianturco, S. Kumar, S. K. Pathak, M. Raimondi, and M. Sironi, Chem. Phys. **215**, 239 (1997).
[11] D. M. Silver, J. Chem. Phys. **72**, 6445 (1980).
[12] C. Møller and M. S. Plesset, Phys. Rev. **46**, 618 (1934).
[13] A. J. McCaffery, Z. T. Alwahabi, M. A. Osborne, and C. J. Williams, J. Chem. Phys. **98**, 4586 (1993).
[14] M. A. Osborne and A. J. McCaffery, J. Chem. Phys. **101**, 5604 (1994).
[15] G. D. Purvis III and R. J. Bartlett, J. Chem. Phys. **76**, 1910 (1982); J. A. Pople, M. Head-Gordon, and K. Raghavachari, J. Chem. Phys. **87**, 5968 (1987).
[16] B. K. Taylor and R. J. Hinde, J. Chem. Phys. (in preparation).
[17] T. H. Dunning, Jr., J. Chem. Phys. **90**, 1007 (1989).
[18] D. E. Woon and T. H. Dunning, Jr., J. Chem. Phys. **100**, 2975 (1994).
[19] D. E. Woon and T. H. Dunning, Jr., J. Chem. Phys. (in preparation).
[20] F.-M. Tao and Y.-K. Pan, J. Chem. Phys. **97**, 4989 (1992).
[21] J. W. Cooley, Math. Comput. **15**, 363 (1961).
[22] Y. C. Chan, D. R. Harding, W. C. Stwalley, and C. R. Vidal, J. Chem. Phys. **85**, 2436 (1986).
[23] E. F. Pearson and W. Gordy, Phys. Rev. **177**, 59 (1969).
[24] A. C. Newell and R. D. Baird, J. Appl. Phys. **36**, 3751 (1965).
[25] J. Vrbik, D. A. Legare, and S. M. Rothstein, J. Chem. Phys. **92**, 1221 (1990).
[26] F.-M. Tao, J. Chem. Phys. **98**, 2481 (1993).
[27] F.-M. Tao, J. Chem. Phys. **98**, 3049 (1993).
[28] G. Chałasiński and M. M. Szczęśniak, Chem. Rev. **94**, 1723 (1994).
[29] R. Burcl, G. Chałasiński, R. Bukowski, and M. M. Szczęśniak, J. Chem. Phys. **103**, 1498 (1995).
[30] S. Shin, S. K. Shin, and F.-M. Tao, J. Chem. Phys. **104**, 183 (1996).
[31] C.-H. Hu and A. J. Thakkar, J. Chem. Phys. **104**, 2541 (1996).
[32] S. F. Boys and F. Bernardi, Mol. Phys. **19**, 553 (1970).
[33] D. Feller, J. Chem. Phys. **98**, 7059 (1993).
[34] D. E. Woon and T. H. Dunning, Jr., J. Chem. Phys. **99**, 1914 (1993).
[35] K. A. Peterson, D. E. Woon, and T. H. Dunning, Jr., J. Chem. Phys. **99**, 1930 (1993).
[36] GAUSSIAN 94, Revision C.2, M. J. Frisch, G. W. Trucks, H. B. Schlegel, P. M. W. Gill, B. G. Johnson, M. A. Robb, J. R. Cheeseman, T. Keith, G. A. Petersson, J. A. Montgomery, K. Raghavachari, M. A. Al-Laham, V. G. Zakrzewski, J. V. Ortiz, J. B. Foresman, J. Cioslowski, B. B. Stefanov, A. Nanayakkara, M. Challacombe, C. Y. Peng, P. Y. Ayala, W. Chen, M. W. Wong, J. L. Andres, E. S. Replogle, R. Gomperts, R. L. Martin, D. J. Fox, J. S. Binkley, D. J. Defrees, J. Baker, J. P. Stewart, M. Head-Gordon, C. Gonzalez, and J. A. Pople, Gaussian, Inc., Pittsburgh, Pennsylvania, 1995.
[37] M. W. Schmidt, K. K. Baldridge, J. A. Boatz, S. T. Elbert, M. S. Gordon, J. H. Jensen, S. Koseki, N. Matsunaga, K. A. Nguyen, S. J. Su, T. L. Windus, M. Dupuis, and J. A. Montgomery, J. Comput. Chem. **14**, 1347 (1993).
[38] HIBRIDON™ is a package of programs for the time-independent quantum treatment of inelastic collisions and photodissociation written by M. H. Alexander, D. E. Manolopoulos, H.-J. Werner, and B. Follmeg, with contributions by P. F. Vohralik, D. Lemoine, G. Corey, R. Gordon, B. Johnson, T. Orlikowski, A. Berning, A. Degli-Esposti, C. Rist, P. Dagdigian, B. Pouilly, G. van der Sanden, M. Yang, F. de Weerd, and S. Gregurick. For more information, see http://www-mha.umd.edu/~mha/hibridon.html.
[39] D. E. Manolopoulos, J. Chem. Phys. **85**, 6425 (1986).
[40] M. H. Alexander and D. E. Manolopoulos, J. Chem. Phys. **86**, 2044 (1987).
[41] P. J. Dagdigian and B. E. Wilcomb, J. Chem. Phys. **72**, 6462 (1980).
[42] See AIP Document No. EPAPS: E-JCPSA6-111-306909 for *ab initio* calculations on which potential energy surface is based. EPAPS document files may be retrieved free of charge from AIP's FTP server (http://www.aip.org/pubservs/paps.html) or from ftp.aip.org in the directory /epaps/. For further information, e-mail: paps@aip.org or fax: 516-576-2223.